

Three Dimensional Simulation of Flow Field around Series of Spur Dikes

Anu Acharya¹, Anil Acharya², and Jennifer G. Duan³

¹Oregon Water Resources Department, Salem, Oregon.

²Assistant Professor, Department of Mechanical and Civil Engineering, Alabama A and M University, Normal,

³Associate Professor, Department of Civil Engineering and Engineering Mechanics, University of Arizona, Tucson, Arizona.

Abstract:- This paper presented a three-dimensional numerical simulation of turbulent flow field around a series of three experimental spur dikes in a flat and a scoured bed surface using FLOW-3D software. At present, none of the turbulence closure model is valid for all cases of turbulent flow in open channels. Some turbulent closures offer advantages over others in specific turbulent flow fields depending on the nature of turbulence.

This study examined one equation mixing length model, standard two-equation $k - \varepsilon$ model, Renormalization

Group (RNG) $k - \varepsilon$ model and Large Eddy Simulation (LES) model. Experimental data from a laboratory study of flow around a series of three dikes in a flat bed and a scoured bed were used to verify the results from the numerical model. Although the simulated mean flow field is close to the experimental data for all the turbulence models, the simulated turbulence properties from different turbulent models deviate considerably.

Modeling results of turbulent kinetic energy using the standard $k - \varepsilon$ model showed over 50% discrepancy from the measurements. The RNG $k - \varepsilon$ model yielded better results of both mean flow field and turbulence kinetic energy for the flat and scoured bed surface. Based on these results, this study recommends the use of RNG $k - \varepsilon$ model for simulating mean flow field around dikes. Further improvements of FLOW-3D model is needed for predicting turbulence properties (e.g. TKE) near this series of spur dikes under various flow conditions.

Keywords:- Numerical models/simulation, Local scour, Spur dike, Turbulence, Sediment transport, Three-dimensional flow.

I. INTRODUCTION

Spur dikes are generally used to protect river banks from erosion or to maintain in-stream hydraulic structures, such as bridges. A single spur dike only change the local flow field. Spur dikes in series are often more effective to stabilize the eroding banks and to re-align the channel. Pools formed due to the local scour around spur dikes can enhance aquatic habitat in unstable streams [1, 2]. Better understanding of the interactions between three-dimensional flow field and bed geometry around spur dikes will benefit the application of spur dikes in river engineering. Over the last few decades, most studies have focused on local scour around river hydraulic structures by physical modeling of bridge piers, spur dikes, and abutments. Since spur dikes and abutments are similar in many aspects, studies on these hydraulic structures are comparable. Investigations on this type of obstruction have been reported extensively [2, 3, 4, 5, 6, 7, and 8]. Those studies reveal that the local scour pattern depends on the complex flow field around bridge piers, channel bed materials, and pier characteristics [9]. Similar to flow field around a vertical circular pier, flow field around dikes is characterized by several vortex systems of different sizes, which are developed due to the presence of the dikes and are considered as the basic mechanism for scour initiation and development [10, 11, 12, 13, 14, and 15]. Though a substantial amount of experimental research on flow field around a single or a series of dike like structures has been completed [16, 17, 18, and 19] flow hydrodynamics, especially turbulence properties, is yet to be fully comprehended.

Most previous studies have examined the impacts on flow field due to groynes orienting at 90° , 45° , 135° and 150° to the flow [9, 20, 21, and 22]. The local scour is initiated as the shear stress exceeds the critical shear stress of sediment transport [2]. The three-dimensional flow field around a series of spur dikes is complex because of the interactions between flow and sediment transport as the scour hole develops. Accurate prediction of scour depends on accurately resolving the flow turbulence structure and sediment transport field

[23]. Methods for predicting three-dimensional flow field and local scour have been developed through the application of three-dimensional hydrodynamic models [24]. [25] used a steady state Navier-Stokes solver coupled with a sediment transport algorithm to simulate the growth of a scour hole around a circular pier and concluded that "three-dimensional numerical models may be able to calculate the scour around an obstacle in a general complex geometry." Since the early work of [25], several numerical models have been developed and used to calculate the three-dimensional flow field around different river hydraulic structures [9, 22, 24, 25, 26, 27, 28, 29, 30, 31, 32, 33, 34, and 35]. With the advancements in computing technology, Computational Fluid Dynamics (CFD) analysis has emerged as a powerful hydraulic design tool [36]. The recent developments in computer software have advanced the use of CFD models to analyze flow field around the spur dikes. A robust three-dimensional hydrodynamic model FLOW-3D has been selected for this study purpose.

Several turbulence closure models have been used in simulating three-dimensional flow fields around spur dikes and bridge piers. [23] used the $k - \epsilon$ turbulence closure model to solve three-dimensional flow around circular piers and computed the associated bed shear stress. [37] found a large discrepancy between the experimental data and his numerical model results showing inadequacy of the $k - \epsilon$ turbulence model for three-dimensional flow. [31] compared the results of the large eddy simulation (LES) and the standard $k - \epsilon$ turbulence model for three-dimensional flow around a cylinder over a scoured bed and confirmed the accuracy of the $k - \epsilon$ model. The RNG model of [38] is an extension of $k - \epsilon$ model that requires less reliance on empirical constants and provides better solutions in areas affected by high shear flow [38]. [39] improved the RNG model by systematically removing the smallest scales of turbulence and calculating their effect on the remaining flow scales. [22, 24, and 34] showed that the RNG $k - \epsilon$ model performs well for simulating flows of extensive separations and recirculation. The goal of this research is to examine the accuracy of various turbulence models for simulating the three-dimensional flow field around the spur dikes on a flat and scoured bed surface. The simulated results from the model are validated with the laboratory data obtained from the University of Arizona. This paper summarizes the experiments, model equations, turbulence closure, computational domain, and simulation results. The simulated results of mean flow velocities in three directions and turbulent kinetic energy are compared with the experimental measurements.

II. EXPERIMENTAL PROCEDURE

The experiments were conducted in a recirculation flume 12.2 m long, 0.6 m wide, and 1.2 m deep located at the courtyard of Civil Engineering and Engineering Mechanics, University of Arizona. The channel sides were of painted metal with a 3m long smooth glass observation section on the right wall of the flume. Three spur dikes of 30 cm length, 4-mm thickness and 40 cm height were protruded from the left-wall of the channel facing upstream at an angle of 150^0 with a distance of 30 cm in between. The first angled dike was located at 1.8 m downstream of the flume inlet. The origin of the Cartesian coordinate was set at the intersection of the bed surface before scouring occurs, the flume right wall, and 0.63 m upstream of the tip of the first spur dike [Fig. 1(a)]. A broad-crested weir of 10 cm height was placed at 10.6 m downstream of the inlet. A valve was used to maintain the required mean water depth of 20 cm at the weir with the height of water above weir as 10 cm. The weir equation is $Q = KLH^{1.5}$, where L is the crest length, H is the height of water flowing over the weir, and K is some constant, was used. For this study, $K = 6678$ (for units of m^3/hr). The total discharge at weir was $0.035 m^3/s$.

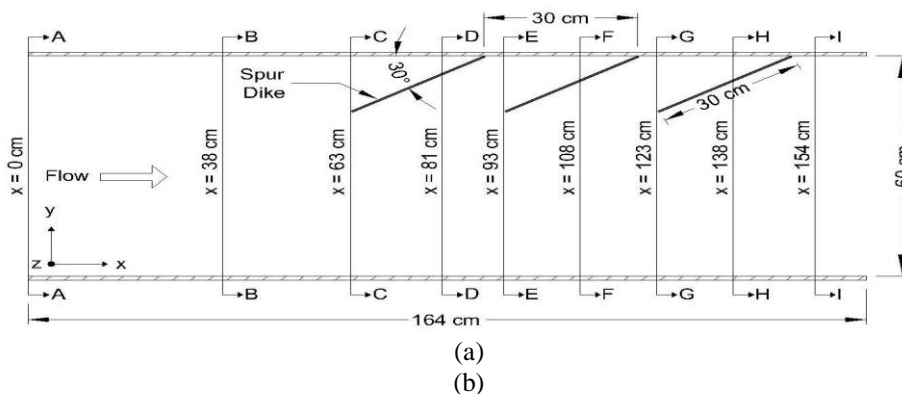


Figure 1. (a) Plan view of experimental setup (b) Diagram of the experimental section showing the relative position of spur dikes and the velocity profile measuring locations.

A 16MHz Sontek microADV was used to measure instantaneous velocity field. The acoustic sensor consists of one transmitter and three receivers. The receivers are aligned to intersect with the transmit beam at a small sampling volume located about 5cm away from the probe in order to reduce the interference with the flow. The control volume of Sontek ADV is a cylinder of diameter 4.0 mm and height of 5.6 mm. The microADV was attached to a point gauge fixed on an instrument cart that was mounted on horizontal steel rails and moved on wheels. The ADV was moved manually in all three directions to measure flow velocities at any location in the cross sections. Flow velocity data at each point were collected at 25 Hz for 4-5 minutes duration for 5,000 instantaneous velocities. Experiments were carried on for both flat fixed bed surface and mobile bed surface with 10 cm thick of a well-sorted sand and gravel mixture. The median grain diameter of sediment is 0.85 mm. The duration of the experimental run was 24 hours to allow the local scour reach an asymptotic state. After the scoured bed reached the equilibrium state, bed sediment was immobilized with a thin layer of cement from 0.50 m downstream of the channel inlet to the weir section for measuring flow field.

The study reach was divided into 41 cross sections. Flow velocities were measured at 304 locations on the x-y plane as shown in Fig. 1(b). The turbulent flow field around the dikes was measured in a grid; starting at 5 mm from the bed, 10 cm from the left wall and extending to 10 cm from the right wall [Fig 1(b)]. The measurement grid was arranged such that the nodes were denser around the dikes and becoming sparser away from the dikes. At each location, velocity measurements were made at ten vertical positions: $z = 0.5, 1.5, 2.5, 3.5, 4.5, 5.5, 6.5, 7.5, 8.5$ and 9.5 cm, which results in a total set of 3,040 point-velocity measurements. All velocity records were processed using the public domain software WinADV to obtain the signal-to-noise ratios (SNR). The signal-to-noise ratio (SNR) is a measure of the relative quality of the acoustic signal received by the ADV whose value should be at least higher than 15 when measuring turbulence [40]. Measurements were filtered using WinADV to reject points with a SNR less than 20. In the present study, 80% or more of the data was above this cutoff value. The approach bed-shear velocity was calculated from the measured velocity profile

at 63 cm upstream from the tip of the first spur dike and in the center of the channel. The shear velocity, $u^* = 1.30$ cm/s, and zero velocity level, z_0 , were determined by fitting logarithmic velocity profile and assuming the von Karman constant as 0.41. The mean velocity of approaching flow was 29.10 cm/s.

III. MODEL

The CFD model selected for this study is the commercially available software ‘FLOW-3D’ [41], which simultaneously solves the three dimensional, transient Navier-Stokes equations on a structured grid. Flow-3D involves very little approximation with the exception of turbulent closure parameterizations to model internal stresses [42]. A detailed description of FLOW-3D can be found in FLOW-3D User’s Manual V9.4 [41]. The program is based on the fundamental laws of mass, momentum and energy conservation and applicable to almost any type of flow process. This model is capable of fluid-boundary tracking by resolving fluid-fluid and fluid-air interfaces with rectangular non-boundary fitted coordinates. This model has been used for various hydraulic and coastal engineering applications, such as flow and scour around a bridge pier [24], flow over a sharp-crested weir, and the near shore transformation of waves [43,44]. The model also has a number of other features including the ability to construct non-uniform grids, automatic time-step selection, graphical post processing, etc. It utilizes a finite difference solution scheme and is able to calculate solutions using various implicit and explicit solver options. FLOW-3D uses a simple grid of rectangular elements. Therefore, it has the advantages of easy mesh generation, regularity for improved numerical accuracy, and minimal memory storage requirement. Geometry is defined within the grid by computing the fractional face areas and fractional volumes of each element that are blocked by obstacles. The use of a multiple and nested meshes, and the re-run capability available in FLOW-3D software, are other options that make the numerical model suitable for hydraulic structure modeling.

The governing equation is the Navier-Stokes equation for incompressible flows as follows:

$$\frac{\partial}{\partial x_i} (u_i A_i) = 0 \tag{1}$$

$$\frac{\partial u_i}{\partial t} + \frac{1}{V_f} \left(u_j A_j \frac{\partial u_i}{\partial x_j} \right) = -\frac{1}{\rho} \frac{\partial P}{\partial x_i} + G_i + f_i \tag{2}$$

Where u_i = mean velocity; P = pressure; A_i = fractional area open to flow in the i direction; V_f = fractional volume open to flow; f_i represents the viscous accelerations; G_i represents the body accelerations.

For a variable dynamic viscosity μ , the viscous accelerations f_i are:

$$\rho V_f f_i = \tau_{w,i} - \left\{ \frac{\partial}{\partial x_j} (A_j \tau_{ij}) \right\} \tag{3a}$$

$$\tau_{ij} = S_{ij} = -\mu_{tot} \left(\frac{\partial u_i}{\partial x_j} + \frac{\partial u_j}{\partial x_i} \right) \quad \tau_{ii} = S_{ii} = -2\mu_{tot} \left(\frac{\partial u_i}{\partial x_i} \right) \tag{3b}$$

where S_{ij} = strain rate tensor; $\tau_{w,i}$ = wall shear stress; ρ = density of water; μ_{tot} = total dynamic viscosity,

which includes the effects of turbulence $\mu_{tot} = \mu + \mu_T$; μ = dynamic viscosity; and μ_T = eddy viscosity.

For non-transport turbulence closure schemes (e.g., LES models), the wall shear stress, $\tau_{w,i}$, is computed as:

$$\tau_{w,i} = \frac{(\mu + \rho a u k_s) u}{d} \tag{4}$$

Where u = parallel component of the velocity computed adjacent to the wall; d = normal distance of the computed velocity from the wall; a = a constant equal to 0.246; and k_s = roughness height. The wall boundary conditions are evaluated differently depending on the turbulence closure scheme. In two equation turbulence closure schemes (e.g., RNG $k - \epsilon$ model, standard $k - \epsilon$ model), boundary conditions for turbulent kinetic energy and energy dissipation rate are computed using the logarithmic law of the wall formulation and calculated as:

$$k = \frac{u_*^2}{\sqrt{C_\mu}}, \quad \epsilon = \frac{u_*^3}{\kappa d} \tag{5}$$

where u_* is the local shear velocity determined from the log-law:

$$u = u_* \left[\frac{1}{\kappa} \ln \left(\frac{\rho u_* d}{\mu} \right) + 5.0 \right] \tag{6}$$

where κ = von Karman constant.

Smagorinsky Large Eddy Simulation (LES) model uses the non-transport turbulence closure scheme. The characteristic length scale, L , and the LES kinematic eddy viscosity, ν_T are defined as:

$$L = (\delta x \delta y \delta z)^{1/3} \tag{7}$$

$$\nu_T = (cL)^2 \sqrt{e_{ij} e_{ij}} \tag{8}$$

where c = a constant equal to 0.1- 0.2; e_{ij} denotes the strain rate tensor components given as:

$$e_{ij} = \frac{1}{2} \left(\frac{\partial u_i}{\partial x_j} + \frac{\partial u_j}{\partial x_i} \right) \tag{9}$$

The volume of fluid (VOF) method [45] is employed in FLOW-3D for tracking fluid-air or fluid-fluid interfaces. The VOF method of tracking has the ability to ignore the air surrounding the flowing water and records the volume of fluid in each rectangular cell. This method also allows the numerical model to create a sharp interface between the water and air without using the fine meshes required by other CFD software. The interfaces with solid boundaries are simulated with the fractional area-volume obstacle representation (FAVOR) method [45] for modeling solid obstacles. It allows the program to use fully structured grids that are very easy to generate throughout the entire flow domain. Other CFD programs may require the use of deformed grid to model flow over and around structures. Additionally, it accounts for cells that are not wholly wet or dry by

determining their fractional influence on the flow. Because of those advantages, relative good representations of flow of complex geometries can be obtained from comparatively coarse meshes. In this study, the three angled dikes were resolved nicely by this method. Most of the terms in the equations are evaluated using the current time-level values of the local variables in an explicit fashion, though a number of implicit options are available.

FLOW-3D supports several turbulent closures using a number of advanced and widely accepted numerical schemes [42,46,47,48]. These include Prandtl's mixing length, one equation turbulent energy (k), the two-equation $k - \varepsilon$, Renormalization Group (RNG), and Large Eddy Simulation (LES) closure schemes. For flow field around dikes, an advanced turbulence closure model is required. The kinematic turbulent viscosity is related to the turbulent kinetic energy, k , and the turbulent dissipation, ε , via the Kolomogorov- Prandtl expression [41]

$$\nu_T = C_\mu \frac{k^2}{\varepsilon} \tag{10}$$

The closure transport equations for turbulent kinetic energy, k , and turbulent dissipation rate, ε , are given by

$$\frac{\partial k}{\partial t} + u_i \frac{\partial k}{\partial x_i} = \frac{\partial}{\partial x_i} \left(\frac{\nu_t}{\sigma_k} \frac{\partial k}{\partial x_i} \right) - \nu_t \left(\frac{\partial u_i}{\partial x_j} + \frac{\partial u_j}{\partial x_i} \right) \frac{\partial u_i}{\partial x_j} - \varepsilon \tag{11}$$

and

$$\frac{\partial \varepsilon}{\partial t} + u_i \frac{\partial \varepsilon}{\partial x_i} = \frac{\partial}{\partial x_i} \left(\frac{\nu_t}{\sigma_\varepsilon} \frac{\partial \varepsilon}{\partial x_i} \right) - C_{1\varepsilon} \frac{\varepsilon}{k} \left[\nu_t \left(\frac{\partial u_i}{\partial x_j} + \frac{\partial u_j}{\partial x_i} \right) \frac{\partial u_i}{\partial x_j} \right] - C_{2\varepsilon} \frac{\varepsilon^2}{k} \tag{12}$$

The empirical constants for the standard $k - \varepsilon$ model are:

$$C_\mu = 0.09, C_{1\varepsilon} = 1.44, C_{2\varepsilon} = 1.92, \sigma_k = 1.0 \text{ and } \sigma_\varepsilon = 1.30$$

The original turbulence model [39] using renormalization group (RNG) theory, results in a model similar to the standard $k - \varepsilon$ model, but with different values for the constants. An extra production term for ε was added in a modification by [49]. However, equation constants that are defined empirically in the standard $k - \varepsilon$ model are derived explicitly in the RNG model. These differences result in greater dissipation of turbulence in areas of strong shear strain, and therefore lead to reduction in eddy viscosity that improves velocity predictions. The empirical constants for RNG $k - \varepsilon$ model are:

$$C_\mu = 0.085, C_{1\varepsilon} = 1.42, \sigma_k = 0.7194, \sigma_\varepsilon = 0.7194$$

where $C_{2\varepsilon}$ is computed from the turbulent kinetic energy (k) and turbulent production

$$\left(\nu_t \left(\frac{\partial u_i}{\partial x_j} + \frac{\partial u_j}{\partial x_i} \right) \frac{\partial u_i}{\partial x_j} \right)_{\text{terms}}$$

To initialize the model, volume flow rate, mean approach velocity of 0.29 m/s, and flow depth of 0.25 m in z-direction were entered at the inlet of the channel. The boundaries bordering the dikes were assumed to have a no-slip rough surface. The roughness values for the flume and the bed for these simulations was 0.00085 m. The inflow boundary was assumed to have a known uniform velocity. An outflow boundary with no re-entry of the fluid condition was used at the downstream boundary. Wall boundary was applied to the bed and side walls, which were defined as no-slip conditions. Boundary condition at the water surface was specified as pressure boundary with the fluid fraction equal to zero.

Grid sensitivity was performed to determine the grid size for the analysis. Cell sizes varied from 1 mm to 5 cm for the analysis purpose. The analysis showed that the finer meshes predicted better results in comparison to coarse meshes. However, the results did not change when the cell sizes were reduced lower than 5 mm. To save the computation time, a computational mesh of 3 mm was constructed within a rectangular coordinate system (Fig. 2) for the analysis purpose. The grid size was selected based on the grid sensitivity analysis which showed that the results wouldn't have been better had the grid sizes been finer.

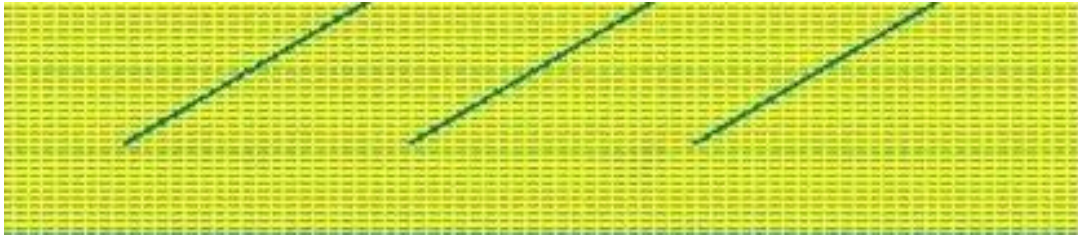


Figure 2. Computational mesh near a series of spur dikes in FLOW-3D

The spur dikes were created as the solid objects and inserted into the domain at the appropriate locations as in the experimental setup. The grid size provided adequate discretization of the spur dike geometry. 40 vertical layers were used in the vicinity of spur dikes. Fig.3 and Fig.4 show the bed bathymetry of the developed scour hole from the experiment.



Figure 3. Picture of scoured bed surface at the equilibrium state

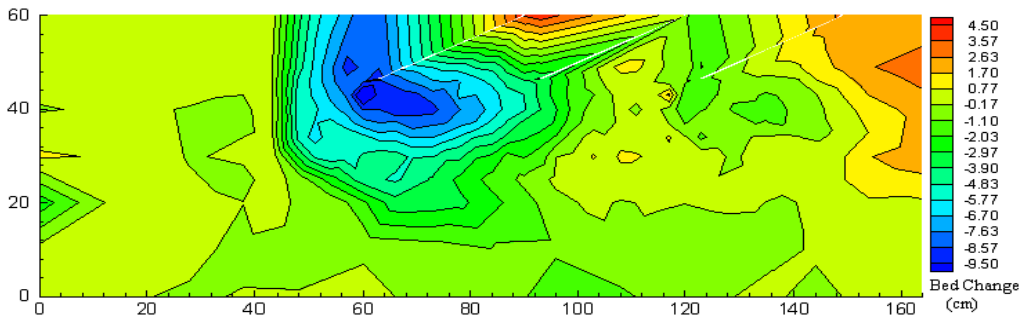


Figure 4. Bed bathymetry of the developed scour hole at $Q = 0.035 \text{ m}^3/\text{s}$

All the simulations were run for a long period until the flow field reached the steady state. FLOW-3D uses explicit time stepping and adjusts the time step continuously during the computation. After the turbulence flow field reached steady state, the changes of the volume of fluid, mean kinetic energy, and average turbulent kinetic energy was less than 2% resulting the steady state solutions. Results from each simulation were used to compare with the experimental measurements. In all calculations, default values of the various turbulence model coefficients were used. Simulations were performed for the initial flat bed and scoured bed cases. In the present investigation, a comparative study of three different turbulence models, RNG $k - \epsilon$, standard $k - \epsilon$ and LES models was made to analyze flow field around the spur dikes and the simulated results are compared with the experimental measurements.

IV. RESULTS AND DISCUSSIONS

Simulated results of mean flow and turbulence for the plane and scoured bed cases were compared with the experimental measurements to evaluate the accuracy of different turbulence closure models in reproducing the three dimensional flow field around a series of spur dikes. The laboratory experiment on the fixed plane bed was carried out by [50], in which detailed measurements of flow field were conducted around a series of spur dikes, subjected to a constant flow depth of 20 cm using the ADV. [50] measured the near bed turbulence and the velocity field using the experimental setup and procedure similar to the one performed in this study for the scoured bed surface. The bathymetry of the scoured bed surface was directly imported into the model as the model input. Three turbulence closure schemes: standard $k - \epsilon$ model, the RNG $k - \epsilon$ model and the LES model, were used. In order to compare simulated velocities with the measurements using the ADV, the model output was sampled at the grid cells having measurements. Fig. 5 shows the computed velocity vectors in the

lateral sections: C-C, D-D, F-F and H-H. It is seen that flow is fully three-dimensional in the vicinity of the spur dikes and downward flow develops along the upstream wall of the first dike. Vortical flow is seen to form in front of the spur dikes near the bottom [Fig. 5(a) and 5(b)]. A strong transverse flow towards the left side wall at $y = 30\text{-}50\text{ cm}$ in section C-C can be seen in Fig 5 (a), which is caused by the lateral flow contraction. Further downstream of the 1st dike at section D-D [Fig 5 (b)], F-F [Fig 5 (c)], and H-H [Fig 5 (c)], a clockwise secondary flow circulation (looking downstream) is formed, a typical feature of the flow near dikes.

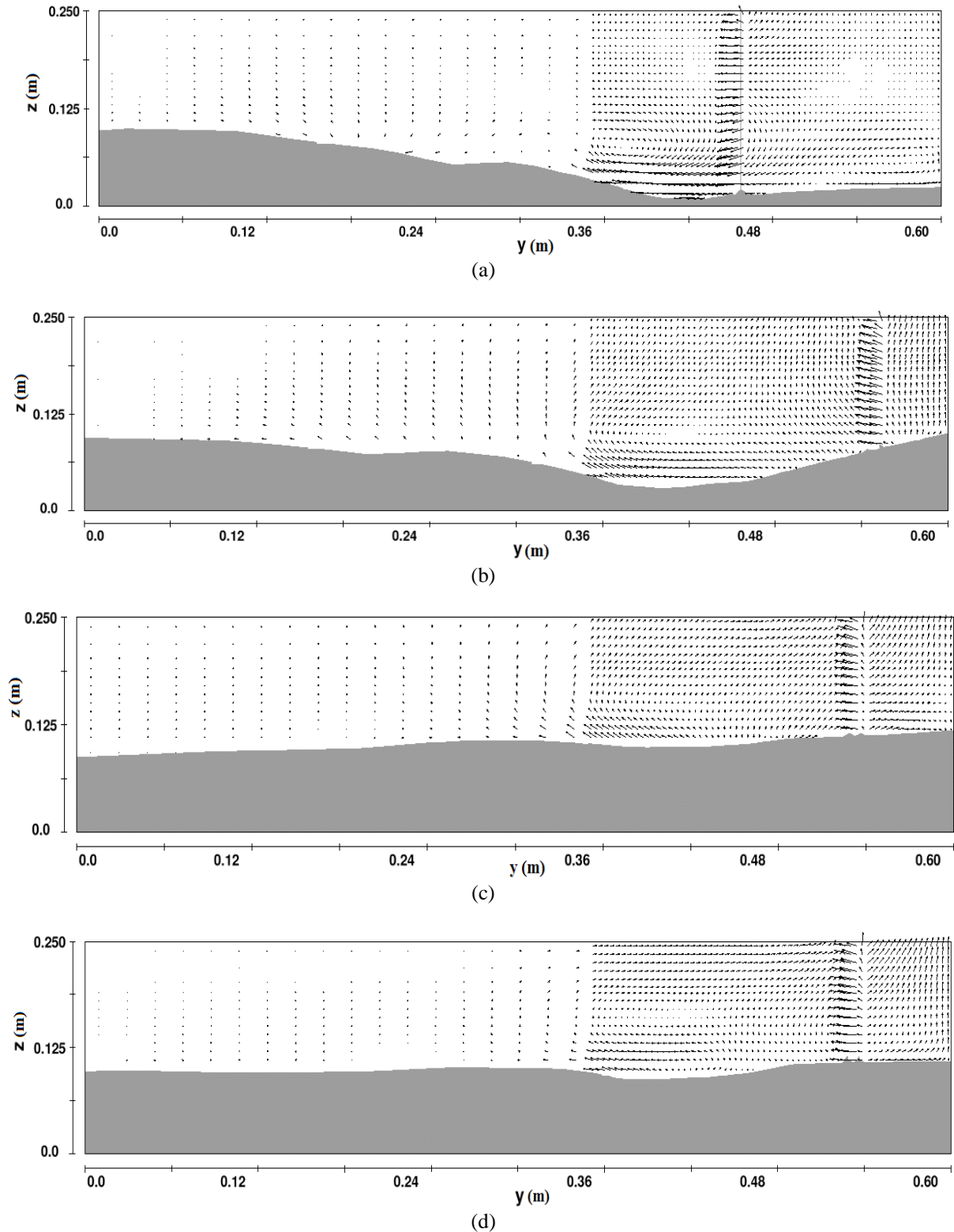
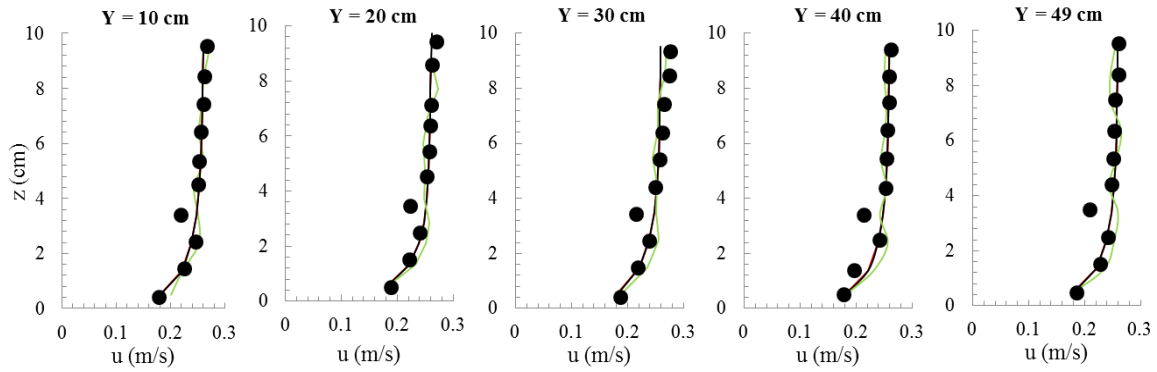


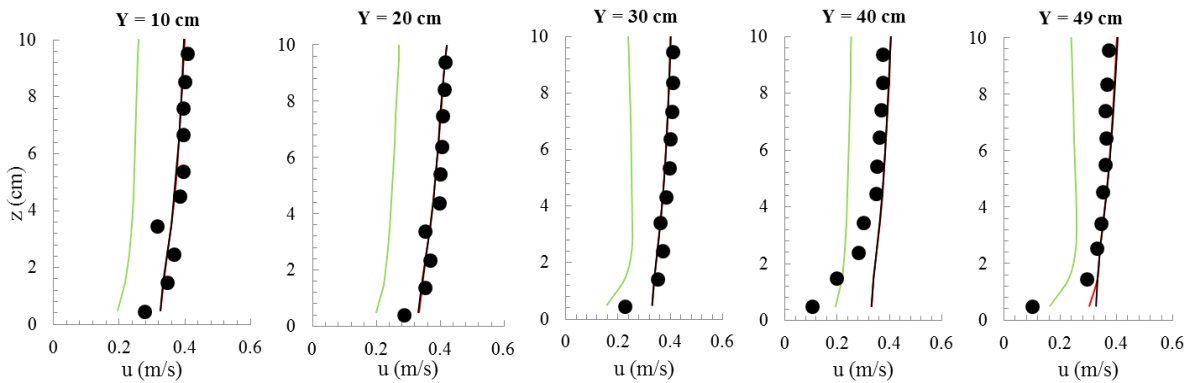
Figure 5. Computed velocity vectors in scoured bed for RNGk- ϵ turbulence closure scheme at different sections (a) C-C (b) D-D (c) F-F and (d) H-H

● Experiment — Standard K-ε — RNG K-ε — LES

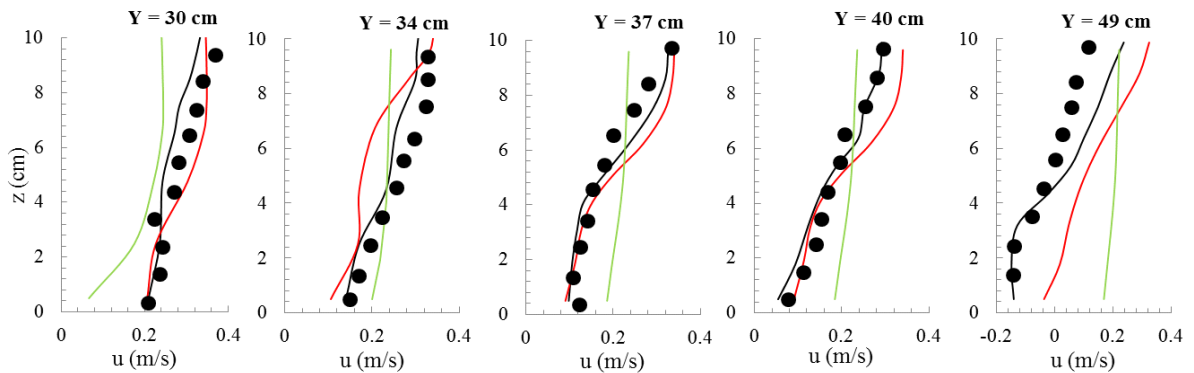
Section A-A



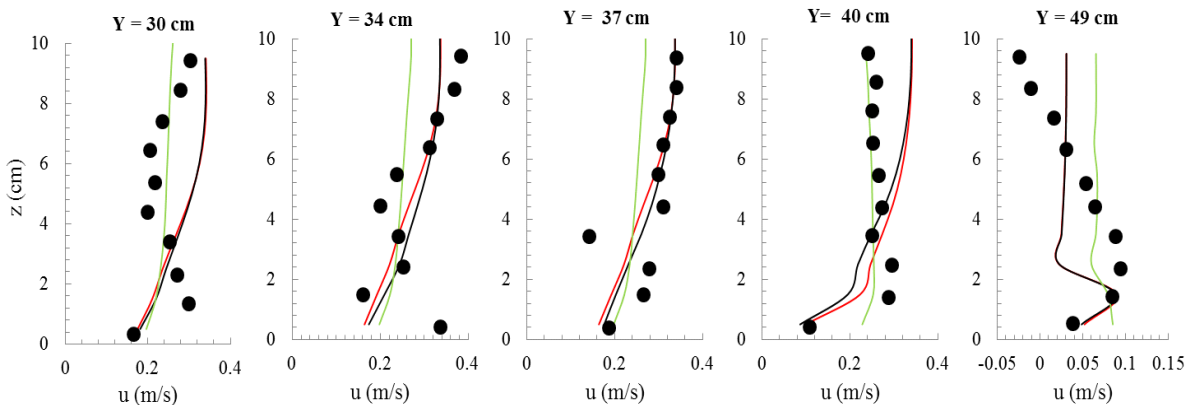
Section B-B



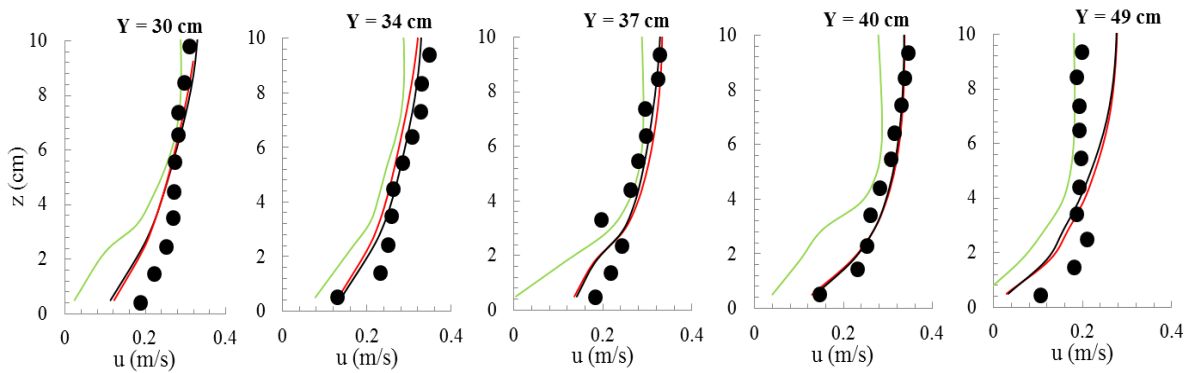
Section C-C



Section E-E



Section G-G



Section I-I

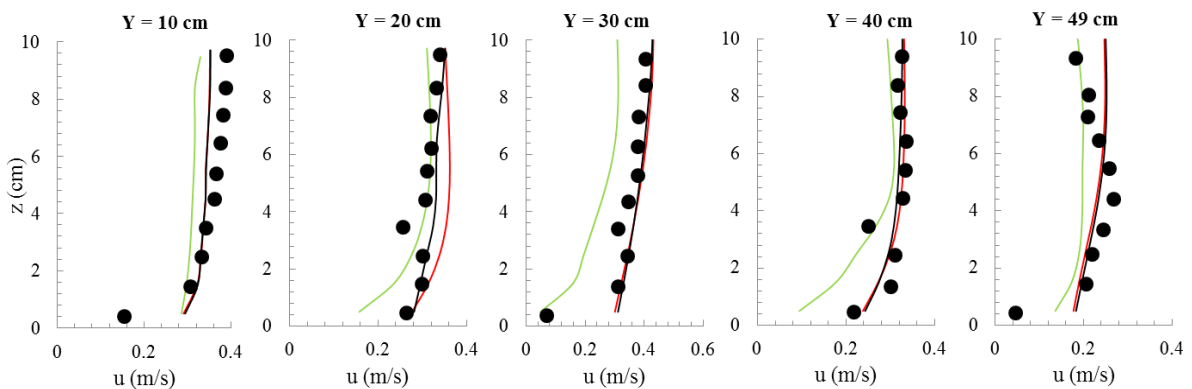
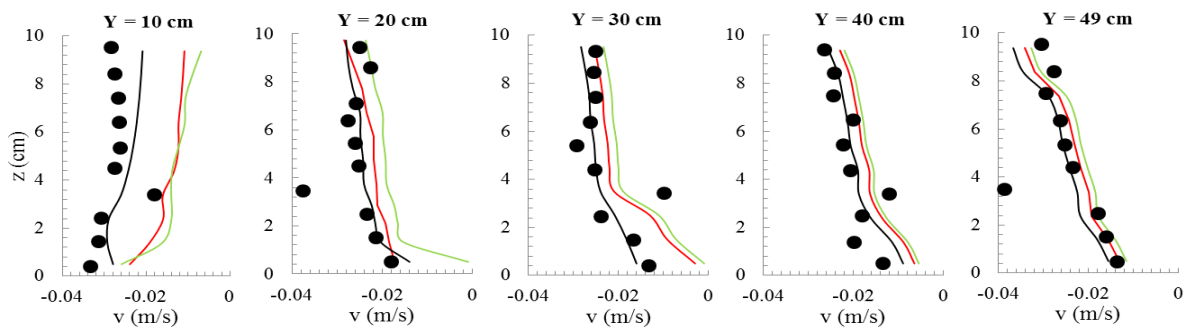


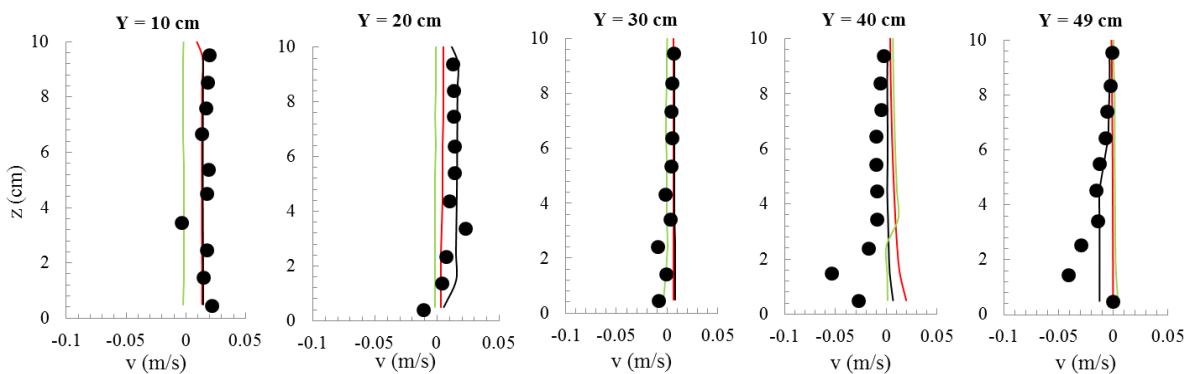
Figure 6. Comparisons of measured (closed and filled circles) and computed longitudinal velocity profiles in scoured bed case for standard $k-\epsilon$, RNG $k-\epsilon$, and LES turbulence closure schemes

● Experiment — Standard K-ε — RNG K-ε — LES

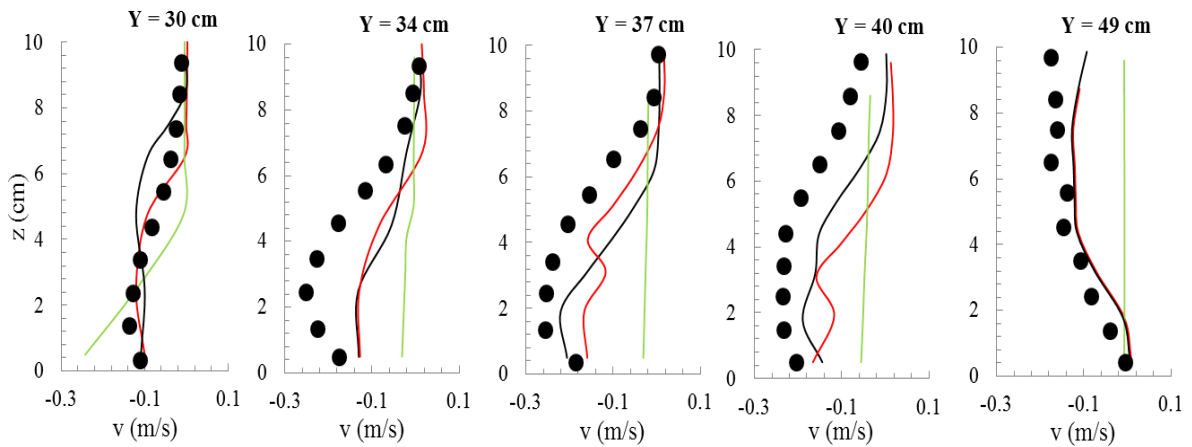
Section A-A



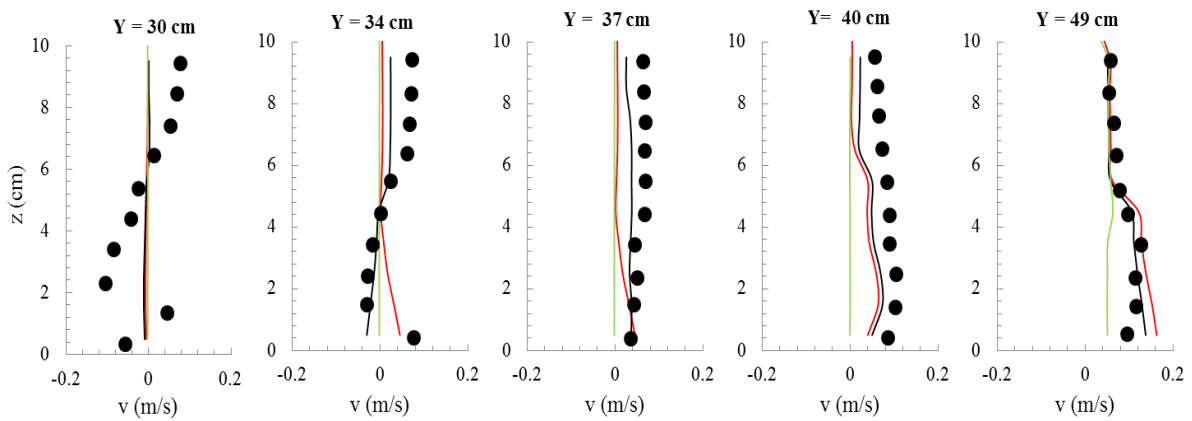
Section B-B



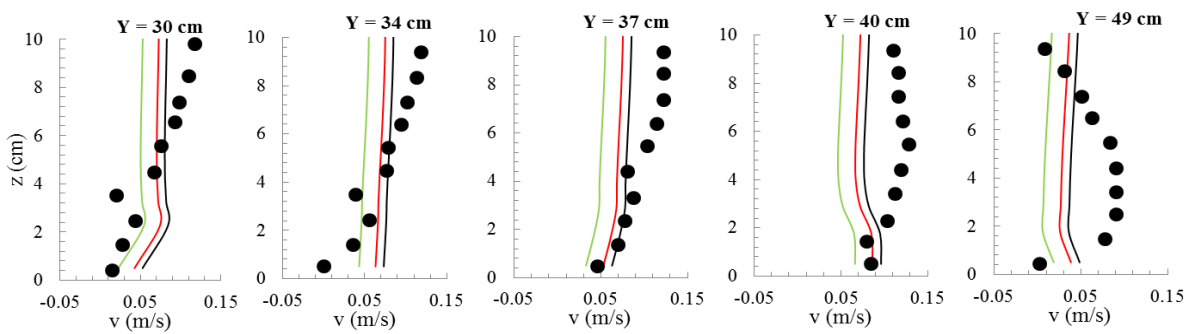
Section C-C



Section E-E



Section G-G



Section I-I

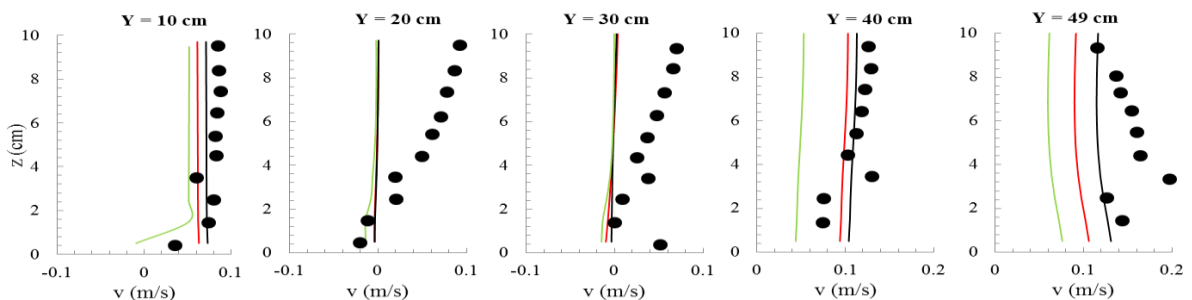
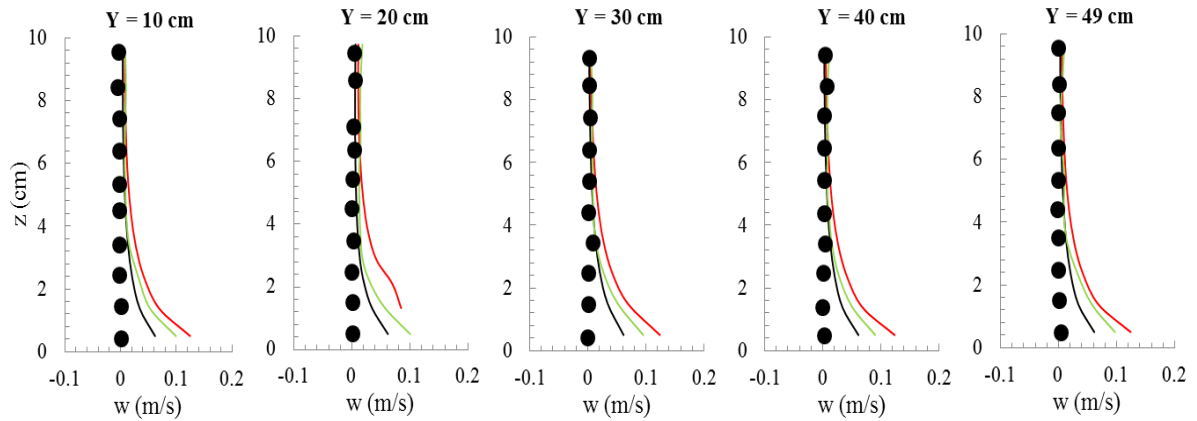


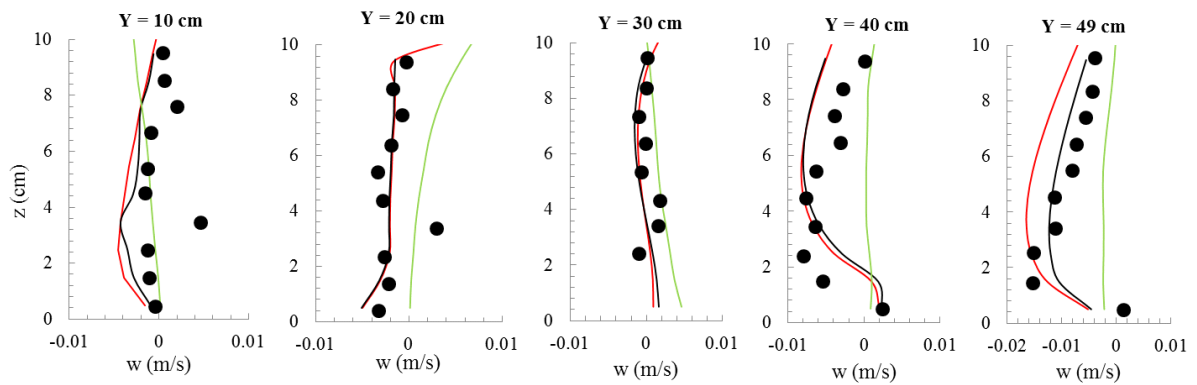
Figure 7. Comparisons of measured (closed and filled circles) and computed transverse velocity profiles in scoured bed case for standard $k-\epsilon$, RNG $k-\epsilon$, and LES turbulence closure schemes

● Experiment — Standard K-ε — RNG K-ε — LES

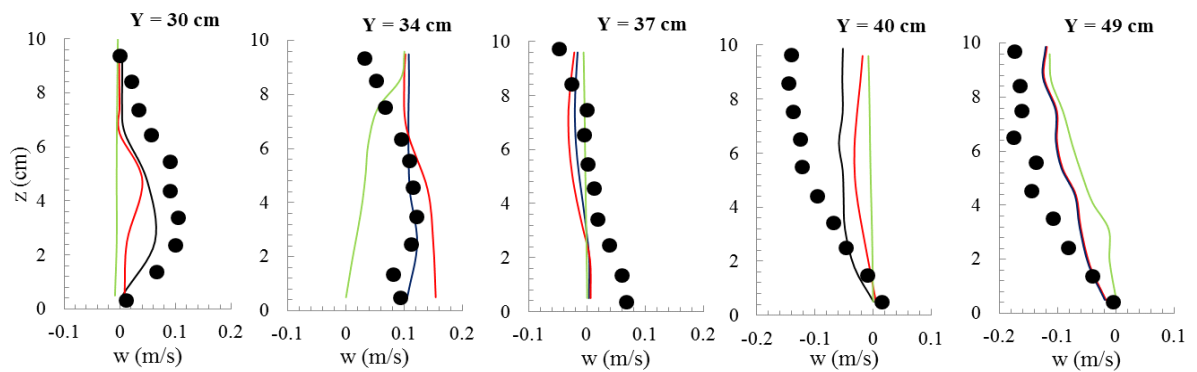
Section A-A



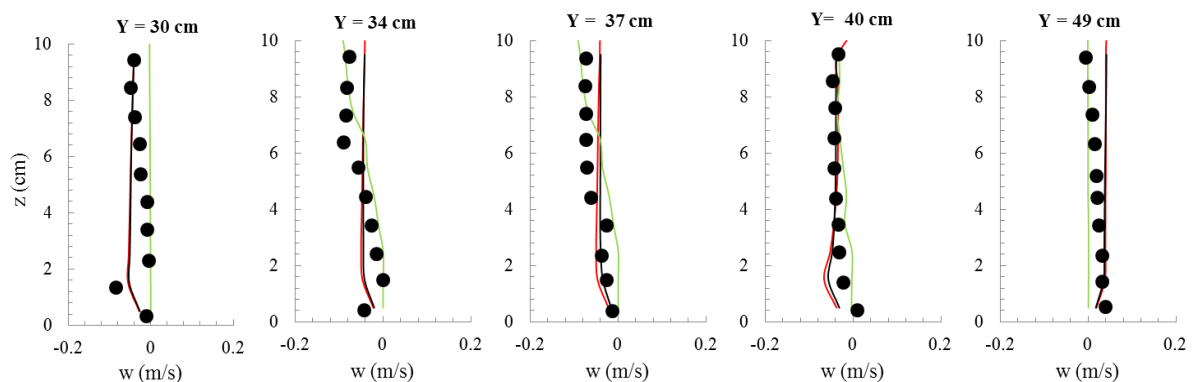
Section B-B



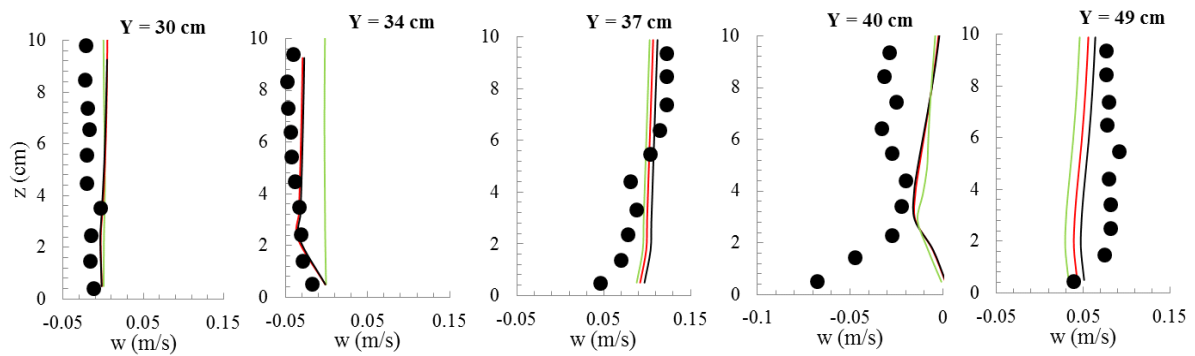
Section C-C



Section E-E



Section G-G



Section I-I

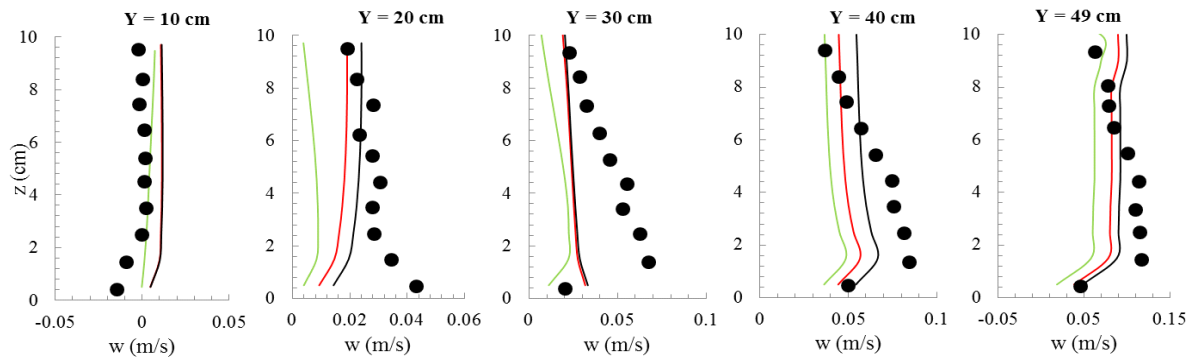
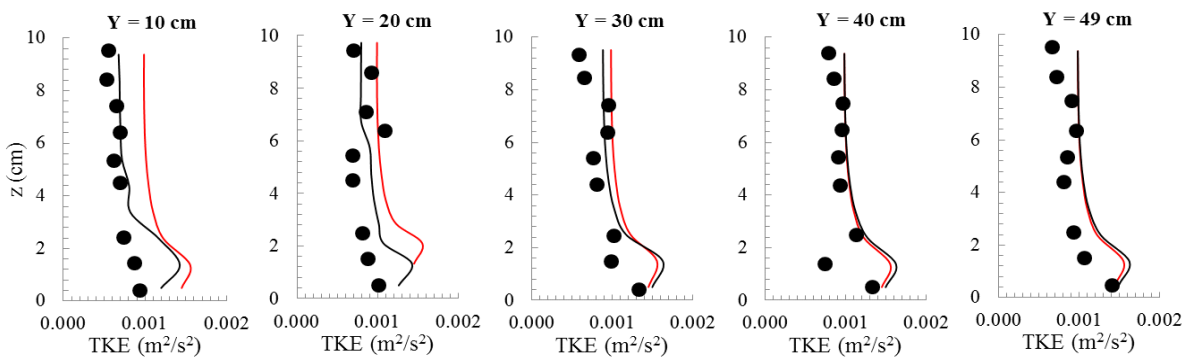


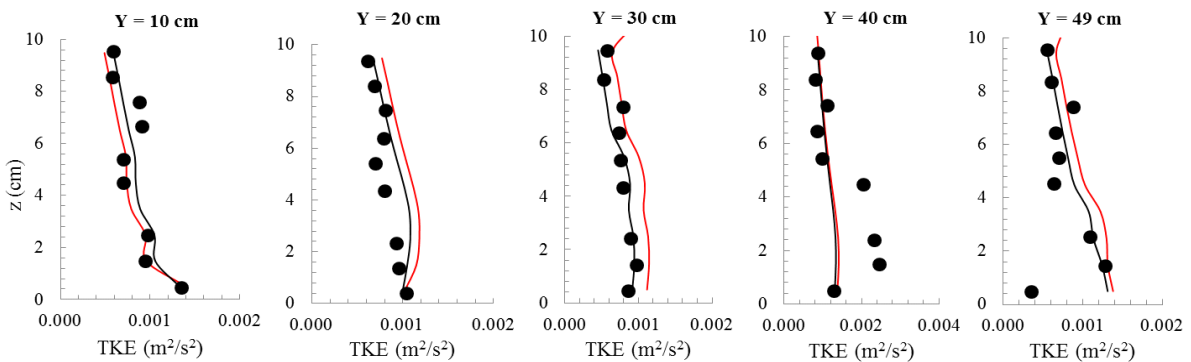
Figure 8. Comparisons of measured (closed and filled circles) and computed vertical velocity profiles in scoured bed case for standard $k-\epsilon$, RNG $k-\epsilon$, and LES turbulence closure schemes

● Experiment — Standard K- ϵ — RNG K- ϵ — LES

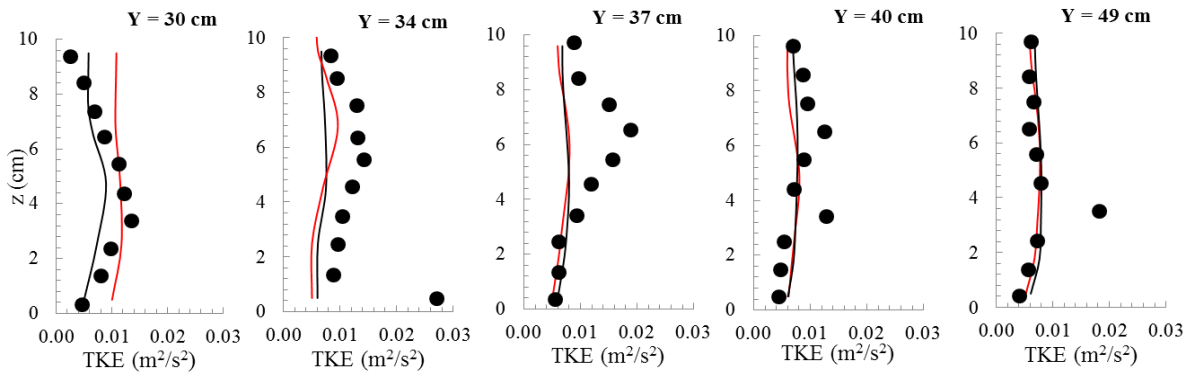
Section A-A



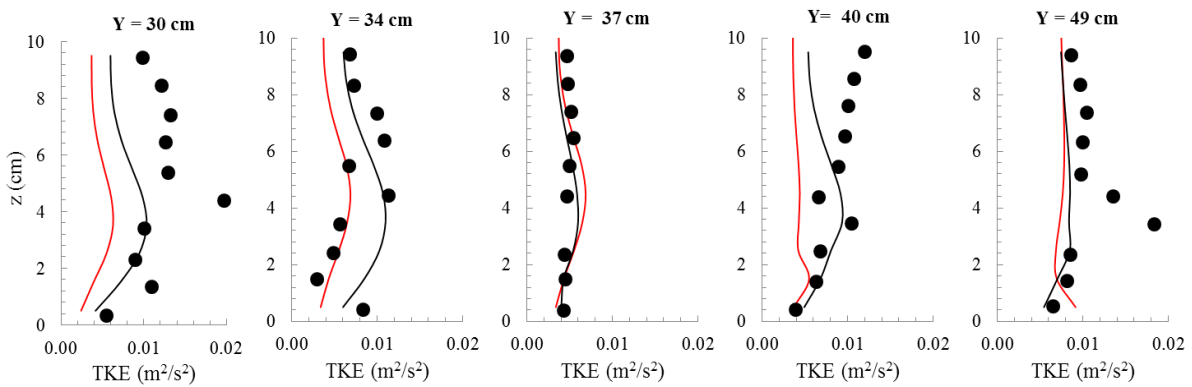
Section B-B



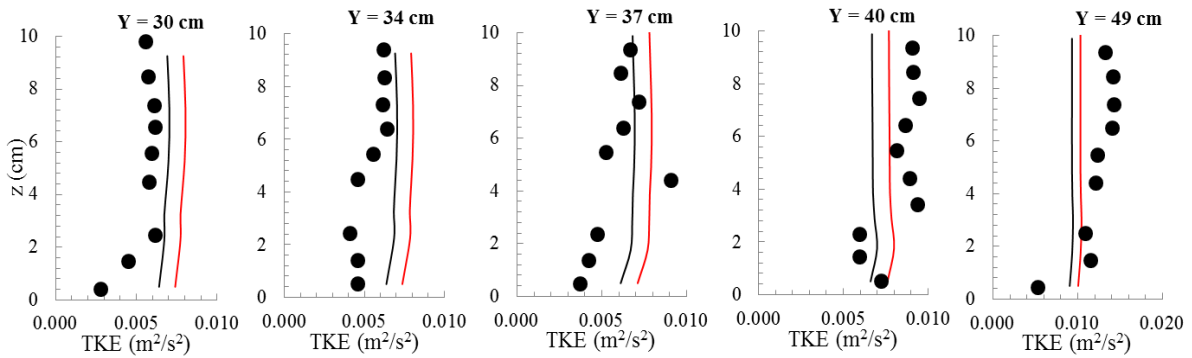
Section C-C



Section E-E



Section G-G



Section I-I

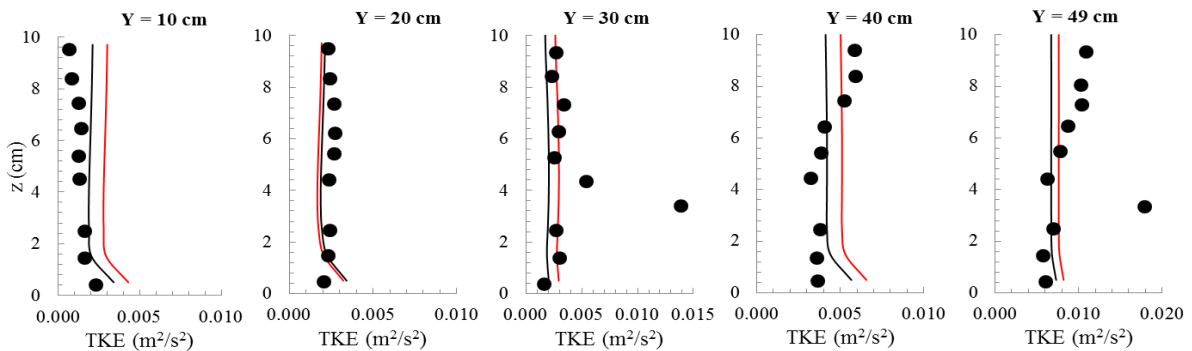


Figure 9. Comparisons of measured (closed and filled circles) and computed Turbulent Kinetic Energy (TKE) profiles in scoured bed case for standard $k-\epsilon$, RNG $k-\epsilon$, and LES turbulence closure schemes

Fig.6, 7, 8 and 9 shows a comparison of the vertical distributions of longitudinal velocity(u), transverse velocity (v), vertical velocity (w) and turbulent kinetic energy (TKE) between the observed and computed results at nine sections from A-A to I-I for the scoured bed. At the approaching flow section A-A, the vertical distributions of the longitudinal velocity, u , obtained using the standard $k-\varepsilon$, RNG $k-\varepsilon$, and LES models fall in a narrow band and agrees with the experimental data (Fig. 6). At section BB, the predicted values of u near the bottom using the standard $k-\varepsilon$ and RNG $k-\varepsilon$ models are higher than the results using the LES model. The LES model underestimates the longitudinal velocity throughout the entire profile. The disagreement is especially pronounced near the bottom and decreases towards the free surface. At section C-C at the tip of the 1st dike, results from the RNG $k-\varepsilon$ model show the closest match with the experimental measurements. Further downstream as the vortical flow fully developed from section D-D to F-F, the results from LES model best match the experimental measurements, whereas the results of u , using the standard $k-\varepsilon$ and RNG $k-\varepsilon$ model, deviate from the experimental values. As flow approaches to the wake region from section G-G to I-I, the result from the RNG $k-\varepsilon$ model best matches the measurements while the results of LES model becomes less accurate. At the approaching flow section A-A, the vertical distributions of the transverse velocity, v , obtained using the RNG $k-\varepsilon$ model also fall in a narrow band and agrees with the experimental data while the standard $k-\varepsilon$ and the LES models over-predicted the experimental data (Fig.7). At section B-B, the predicted values of v near the bottom using the standard $k-\varepsilon$ and RNG $k-\varepsilon$ models predict the results better than those using the LES model. The LES model underestimates the transverse velocity throughout the entire profile up to the middle of the channel and over-estimates the other half. The disagreement is distinct near the bottom and reduces towards the free surface. At section C-C at the tip of the first dike, results from the RNG $k-\varepsilon$ model shows the closest match with the experimental measurements. Further downstream from Section D-D to F-F, none of the models best matches the experimental measurements. The results of v , using the standard $k-\varepsilon$, RNG $k-\varepsilon$ and LES model deviate from the measurements. As flow approaches to the wake region from section G-G to I-I, the results from the RNG $k-\varepsilon$ model best matches the measurements at the bottom layers and the gap widens towards the free surface. The results of LES model also become less accurate. At the approaching flow section A-A, the vertical distributions of the vertical velocity, w , obtained using the standard $k-\varepsilon$, RNG $k-\varepsilon$, and the LES models over-predict the measured data at the bottom layers and agree well with the experimental data towards the surface layers (Fig. 8). At section B-B, the predicted values of w using the standard $k-\varepsilon$ and the RNG $k-\varepsilon$ models are smaller than the results using the LES model. The LES model overestimates the vertical velocity throughout the entire profile. The remarkable disagreement is at the free surface and decreases towards the bottom. At section C-C, the RNG $k-\varepsilon$ model shows better results than the other two models and shows the closest match with the experimental measurements. Further downstream of the vertical flow sections from D-D to F-F, the results from LES model best match the experimental measurements. At the wake region from section G-G to I-I, the results from the RNG $k-\varepsilon$ model best match the measurements at the free surface but deviate towards the bottom. The LES model mostly under-predicts the experimental data in this region.

At the approaching flow section A-A, the vertical distributions of the turbulent kinetic energy, TKE, obtained using the standard $k-\varepsilon$ and the RNG $k-\varepsilon$ models over-predict the experimental data at the bottom and agree well towards the free surface (Fig 9). At section B-B, the predicted values from both models fall in a narrow band and agree with the experimental data. At section C-C at the tip of the first dike, results from the RNG $k-\varepsilon$ model show the closest match with the experimental measurements, but the pronounced disagreement is seen at the middle layers with the model not being able to follow the data trend correctly. Further downstream as the vortical flow fully develops from Section D-D to F-F, none of the models predicts the experimental data correctly. The results from the standard $k-\varepsilon$ and the RNG $k-\varepsilon$ model deviate from the experimental data. As flow approaches to the wake region from section G-G to I-I, the predicted values of TKE using the standard $k-\varepsilon$ model are greater than the results using the RNG $k-\varepsilon$ model. However, The

RNG $k - \varepsilon$ model also overestimates the TKE throughout the entire profile. The disagreement is evident near the bottom and decreases towards the free surface. These results indicated that the RNG $k - \varepsilon$ model is most suitable in the regions of flow contraction and turbulence wake and is not as accurate as the LES model in highly turbulent flow region having strong turbulence concurrent structures.

Table 1. Statistical comparison of the experimental and modeled results for the fixed flatbed case

RNG model					
Parameters	MAE	MSE	RMSE	R ²	R
Longitudinal velocity (u)	0.024	0.001	0.032	0.952	0.976
Transverse velocity (v)	0.032	0.0017	0.042	0.789	0.888
Vertical velocity (w)	0.004	0.00004	0.006	0.187	0.432
Turbulent kinetic energy (m ² /s ²)	0.00156	0.00001	0.002	0.434	0.658
$k-\varepsilon$ model					
Parameters	MAE	MSE	RMSE	R ²	R
Longitudinal velocity (u)	0.084	0.0112	0.106	0.625	0.79
Transverse velocity (v)	0.046	0.0033	0.058	0.716	0.846
Vertical velocity (w)	0.0041	0.00004	0.007	0.012	0.11
Turbulent kinetic energy (m ² /s ²)	0.00297	0.00002	0.004	0.189	0.435
LES model					
Parameters	MAE	MSE	RMSE	R ²	R
Longitudinal velocity (u)	0.087	0.013	0.114	0.282	0.531
Transverse velocity (v)	0.085	0.009	0.094	0.425	0.651
Vertical velocity (w)	0.006	0.002	0.047	0.004	0.063

To compare the simulated results from FLOW-3D using different turbulence closure models, statistical parameters are calculated for the errors between the simulated and measured data as shown in Table 1 and Table 2. Table 1 and Table 2 show the statistical parameters between the predicted and observed mean velocity and turbulent kinetic energy for all three turbulence models used in this study. Table 1 summarizes the results of 304 nodal points measured near the bed, whereas Table 2 includes the results of 3040 points in the scoured bed experiment. Four statistical measures of model predictions are adapted in this study. The first one is R-squared correlation that measures the model’s accuracy in predicting the velocities in three dimensions. Similar tests in the recent literature on CFD applications to open channels [33,34,51] have reported R², the squared correlation between simulated and measured values of flow property. In applications to smooth-walled flumes, R² values up to 0.95 for *u* and 0.75 for *w* have been achieved [52], but results for natural rivers showed worse agreements between modeling results and measurements: R² values of 0.50–0.89 for the horizontal velocity component, and 0.01–0.50 for the vertical component [53,54,55,56].

The model’s accuracy in predicting the velocity magnitudes is evaluated using the mean absolute error (MAE), mean square error (MSE), and root mean square error (RMSE). The MAE, MSE and RMSE are defined as:

$$MAE = \frac{1}{n} \sum_{i=1}^n |O_i - P_i| ; \quad MSE = \frac{1}{n} \sum_{i=1}^n (O_i - P_i)^2 ; \quad RMSE = \sqrt{\frac{1}{n} \sum_{i=1}^n (O_i - P_i)^2} \tag{13}$$

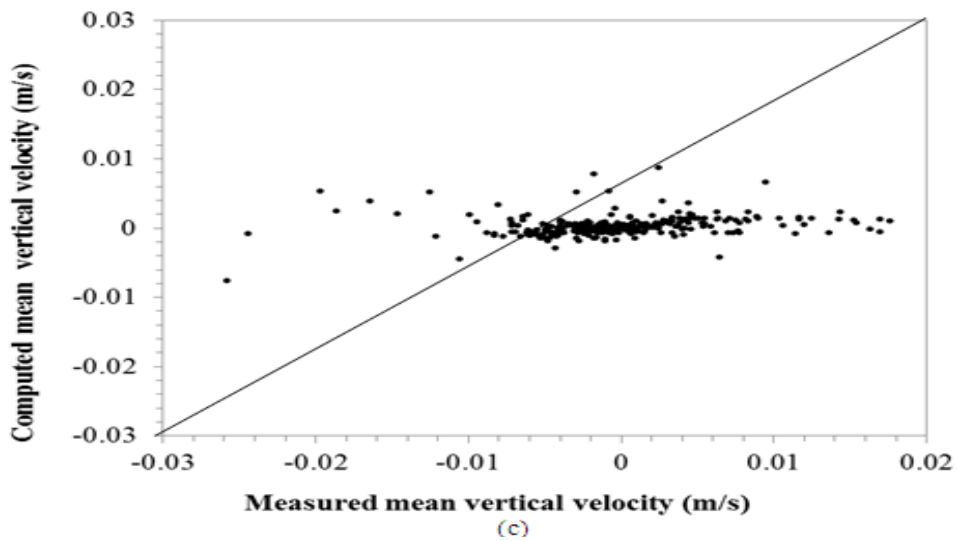
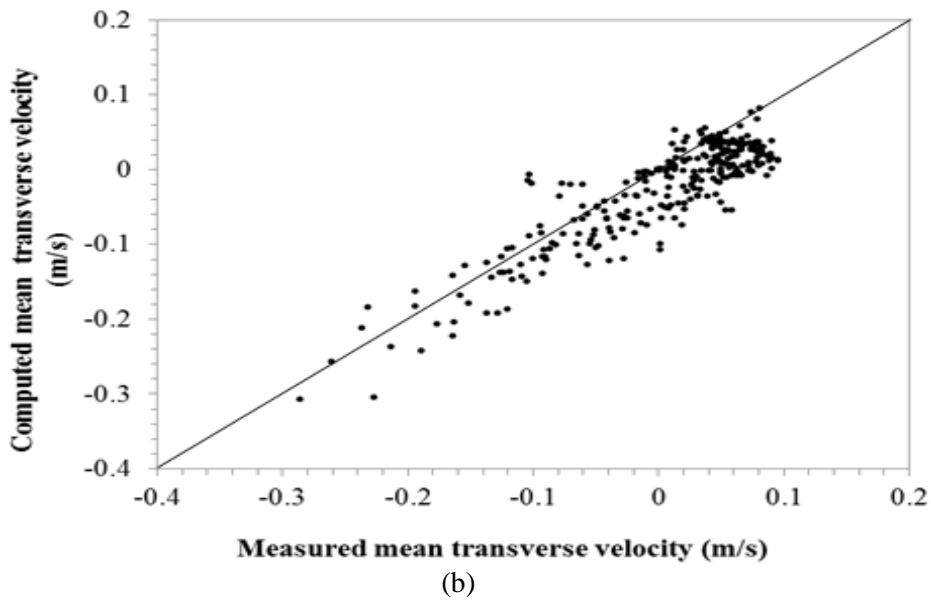
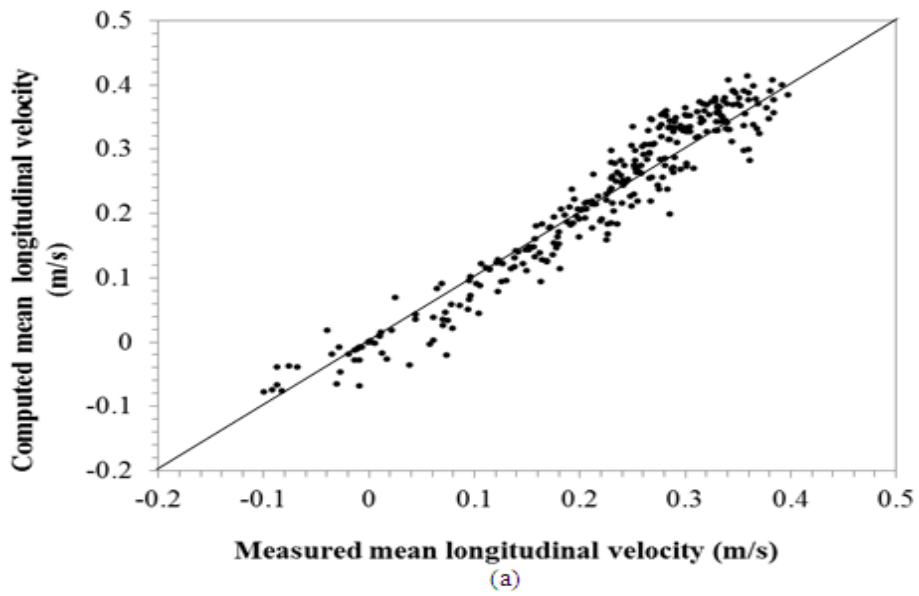
Where *n* = number of velocity data points within each individual longitudinal velocity profile; *O_i* and *P_i* = the observed and predicted values, respectively. The R², MAE, MSE, and RMSE are calculated for the horizontal mean velocity, *u*, the transverse velocity, *v*, the mean vertical velocity, *w*, and the turbulent kinetic energy, TKE.

Table 2. Statistical comparison of the experimental and modeled results for scoured bed case

RNG model					
Parameters	MAE	MSE	RMSE	R ²	R
Longitudinal velocity (u)	0.051	0.005	0.068	0.634	0.796
Transverse velocity (v)	0.026	0.002	0.043	0.795	0.891
Vertical velocity (w)	0.027	0.001	0.036	0.464	0.681
Turbulent kinetic energy (m ² /s ²)	0.002	0.000	0.004	0.384	0.620
<i>k-ε</i> model					
Parameters	MAE	MSE	RMSE	R ²	R
Longitudinal velocity (u)	0.073	0.010	0.098	0.298	0.545
Transverse velocity (v)	0.075	0.008	0.092	0.246	0.495
Vertical velocity (w)	0.037	0.003	0.051	0.220	0.469
Turbulent kinetic energy (m ² /s ²)	0.006	0.000	0.008	0.212	0.460
LES model					
Parameters	MAE	MSE	RMSE	R ²	R
Longitudinal velocity (u)	0.083	0.011	0.105	0.362	0.602
Transverse velocity (v)	0.082	0.010	0.100	0.129	0.359
Vertical velocity (w)	0.034	0.002	0.047	0.144	0.379

The correlation coefficients show an overall good agreement for the longitudinal and transverse velocity, with average R^2 values for the flat and scoured bed case being 0.870 and 0.714, respectively. However, much weaker agreements are found for the vertical component (w) and turbulent kinetic energy (TKE), with R^2 ranging between 0.187 -0.464 and 0.384 -0.434 for w and TKE, respectively. Because of the smaller range of velocities in the vertical component, lower velocity correlations have been seen in most three dimensional CFD studies (e.g., [22, 33,34]. In addition, the lower correlation is also due to differences in the position of the center of the simulation cells compared to the ADV sampling volume. Better agreements (as measured by R^2 ; Table 1 and Table 2) than in most of these previous studies [54,55,56] are obtained, which gives some confidence in the use of the CFD models to identify and describe flow structures.

Comparison of the results from the RNG $k - \epsilon$ model with the standard $k - \epsilon$ model and LES model shows the importance of selecting an appropriate turbulence models in simulating turbulent flow field around spur dikes. The improvement in modeling results using the RNG $k - \epsilon$ model is most evident in the transverse velocities for which the correlation between the predicted and measured values in scoured bed is only 0.495 using the standard $k - \epsilon$ model, 0.359 using the LES model, and 0.891 using the RNG $k - \epsilon$ model (Table 2). Similarly, the correlation is 0.651 using the LES model, 0.846 using the $k - \epsilon$ model, and 0.888 using the RNG $k - \epsilon$ model in the plane bed case (Table 1). In addition, the correlation between simulated and measured vertical velocity is also higher using the RNG $k - \epsilon$ model compared to the standard $k - \epsilon$ model and LES model. The correlation between simulated and measured turbulent kinetic energy for plane bed and scoured bed case using RNG $k - \epsilon$ is 0.658 and 0.620, respectively, which is higher than the standard $k - \epsilon$ model. The simulated turbulent kinetic energies with the standard $k - \epsilon$ model are generally higher than those using the RNG $k - \epsilon$ model, and an inspection of the values shows this is especially true within the recirculation zone.



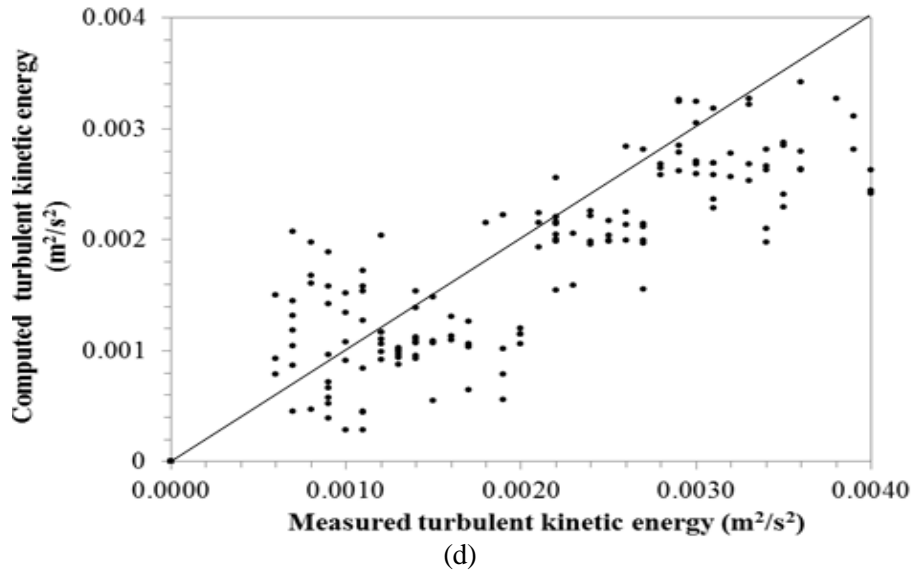
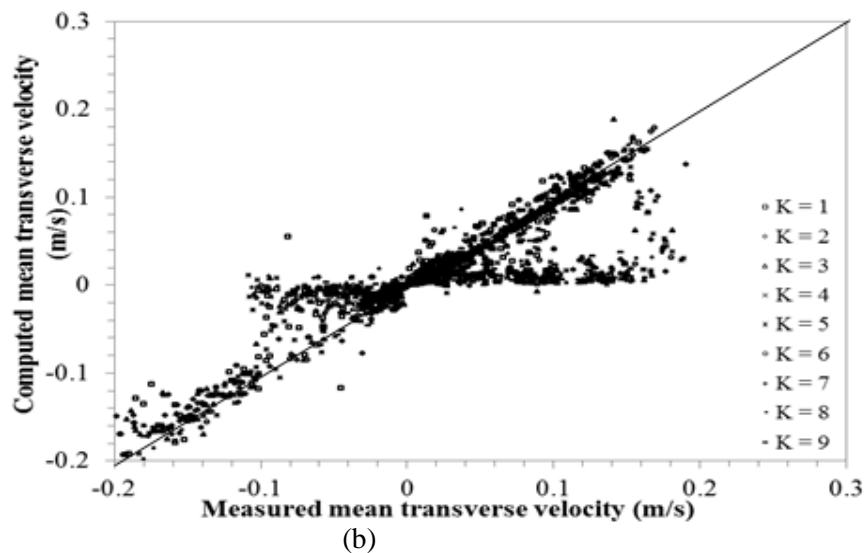
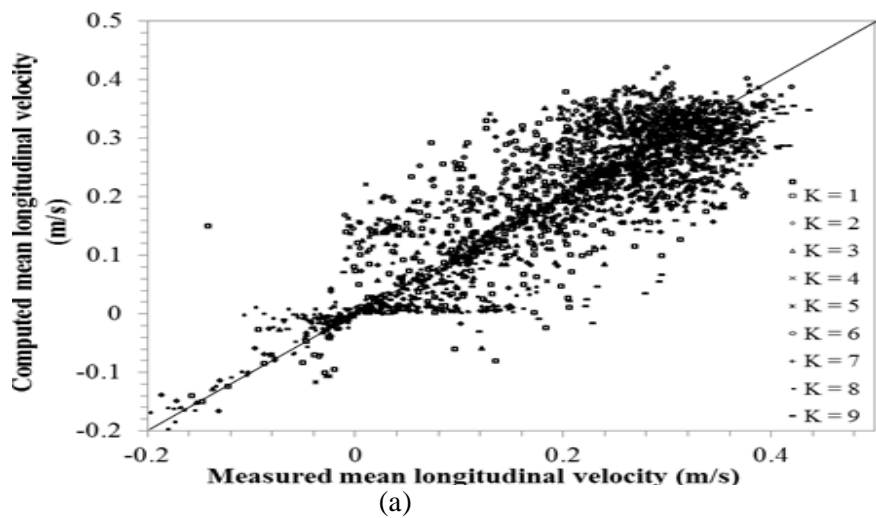


Fig.10. Comparison of simulated results from RNG $k-\epsilon$ model and measured values for fixed flat-bed case: (a) longitudinal velocity; (b) cross-stream velocity; (c) vertical velocity; (d) turbulent kinetic energy



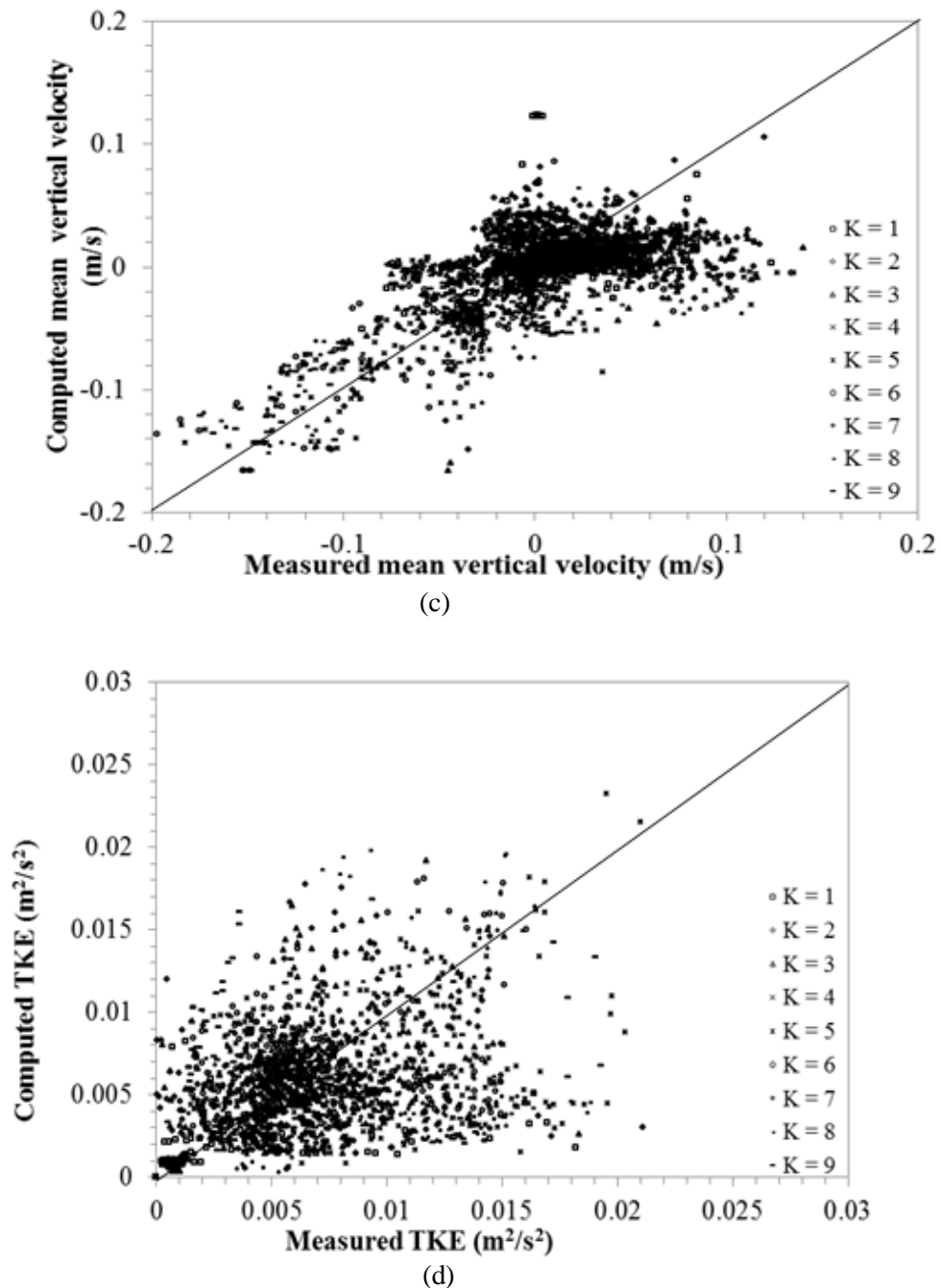


Fig.11. Comparison of simulated results from RNG $k-\epsilon$ model and measured values for scoured bed case: (a) longitudinal velocity; (b) cross-stream velocity; (c) vertical velocity; (d) turbulent kinetic energy. $K = 1, K = 2, \dots, K = 9$ indicate the distance of the velocities above the bed, $K = 1$ represents the level nearest the bed, and $K = 9$ represents the level nearest the water surface

The study implies that the simulated turbulent kinetic energy using the RNG $k-\epsilon$ model are generally lesser than those observed [Fig. 10(d) and 11(d)] and there is a prominent difference in the recirculation zone. The predictions using the RNG $k-\epsilon$ model agree better than other turbulence models for the existing experimental results of flow field around a series of dikes on the plane bed and scoured bed. Using the RNG $k-\epsilon$ turbulence model, the general agreements between model predictions and measured velocity components give sufficient confidence to use the numerical model to investigate the turbulence flow field and scour formation around dikes. Therefore, the RNG $k-\epsilon$ model [57], a widely used turbulence closure model

for incompressible flow, is adopted for the comparative study of the simulated and experimental results for the plane and scoured bed experiments.

Fig.10 and Fig.11 show plots of measured versus predicted values for the simulation using the RNG $k - \varepsilon$ turbulence model. The point velocities from the model match the measured data with very little systematic error in Fig. 10 and 11, although some discrepancies in the recirculation zone are apparent. In the main channel and near the upstreamside of the spur dike, the predicted velocities are very close to those measured. For the simulation with the RNG $k - \varepsilon$ turbulence model, the equations of the regression lines for the longitudinal velocity and transverse velocities are very close to the line of perfect agreement. Although the correlation for the vertical velocity is lower, it is still very reasonable. The lower correlation for the vertical velocity is attributed to ADV measurement errors as it approaches to the bed surface. The correlation for turbulent kinetic energy is much lower, and the highest values are under-predicted by about 50%. Given the success of the model in predicting the mean velocities, the performance of the RNG $k - \varepsilon$ turbulence model appears to be preferable to the standard $k - \varepsilon$ and the LES turbulence model. However, none of the turbulence closure models is accurate in predicting the measurements of turbulent kinetic energy (Lane et al. 1999). The inaccuracies in TKE prediction are caused by the limitations of turbulence closure models and the errors of ADV measurements especially near the bed surface. This result further confirm that the existing turbulence closure models are suitable for predicting mean flow field and limited in predicting turbulence properties (e.g. TKE). Direct simulation of turbulence flow field without any turbulence closure models perhaps will provide better results of turbulence flow field.

V. CONCLUSIONS

This study employed FLOW-3D model to simulate the three-dimensional turbulent flow field around a series of three spur dikes in a flat fixed and a scoured bed. This study examined one equation mixing length model, Prandtl's mixing length model, one equation turbulent energy (k) model, standard two-equation ($k - \varepsilon$) model, RNG turbulence model, and large eddy simulation. Prandtl's mixing length model and one equation turbulent energy (k) model were not used for the detailed analysis due to their inability to simulate the flow field near the dikes effectively.

Experimental data on a flat and a scoured bed were used to verify the results from the numerical model. Although the simulated mean flow field is close to the experimental data, the simulated turbulence properties from different turbulent model deviate considerably. The MSE for the mean longitudinal velocity ranged from 0.001-0.005 for the RNG $k - \varepsilon$ model, 0.010 - 0.011 for the standard $k - \varepsilon$ model and 0.011-0.013 for the LES model. The correlation (R) for mean horizontal velocity ranged from 0.796 to 0.976 for the RNG $k - \varepsilon$ model, 0.545 - 0.790 for the standard $k - \varepsilon$ model, and 0.531 - 0.602 for the LES model. The model predicted quite good estimations of the longitudinal mean velocity regardless of turbulence closure schemes. However, the predictions of vertical velocity showed more variability using different closure schemes. The overall agreement between the simulated and measured velocities is good, with the exception of a systematic discrepancy in areas where the transverse and vertical velocity components are negative. This occurs primarily downstream of the spur dike in the recirculation zone. Although the standard $k - \varepsilon$ model and LES model are considered superior in different studies of three-dimensional flow field, these models performed poorly compared to the RNG $k - \varepsilon$ model in estimating the flow velocity and turbulent kinetic energy around a series of spur dikes. The LES model largely under-estimated the velocity field near the bed, while the results using the standard $k - \varepsilon$ model showed over 50% discrepancy from the measured TKE. The RNG $k - \varepsilon$ model is found to give good results for estimating the longitudinal and transverse velocity field whereas the results are only satisfactory for the vertical velocity field and the turbulent kinetic energy. The results show that the differences between the simulated and experimental values are smaller at the measurement positions further downstream from the dikes (such as 1mm) as flow becomes steady uniform. Since the simulated results of mean flow field qualitatively agree with the experimental data, this study recommends the use of RNG $k - \varepsilon$ model for simulating the mean flow field around the dikes for fixed flat and scoured bed. This study also showed that none of the turbulence closure model was able to predict accurately the turbulence properties (e.g. TKE) near the dikes, improvements in FLOW-3D are needed for better predicting turbulence flow properties by using direct numerical simulation technique.

REFERENCES

- [1] F.D. Shields, Jr., C.M. Cooper, and S.S. Knight, Experiment in stream restoration, *J. Hydraul. Eng.*, 121(6), 1995, 494–502.
- [2] R.A. Kuhnle, Y. Jia, and C.V. Alonso, Measured and simulated flow near a submerged spur dike, *J. Hydraul. Eng.*, 134(7), 2008, 916–924.
- [3] R.J. Garde, K. Subramanya, and K.D. Nambudripad, Study of scour around spur-dikes, *J. Hydraul. Div., ASCE*, 87(6), 1961, 23–37.
- [4] E.M. Laursen, Analysis of relief bridge scour, *J. Hydraul. Div., Am. Soc. Civ. Eng.*, 89(3), 1963, 93–118.
- [5] M.A. Gill, Erosion of sand beds around spur dikes, *J. Hydraul. Div., ASCE*, 98(9), 1972, 1587–1602.
- [6] T.F. Kwan, and B.W. Melville, Local scour and flow measurements at bridge abutments, *J. Hydraul. Res.*, 32(5), 1994, 661–673.
- [7] S.Y. Lim, Equilibrium clear water scour around an abutment, *J. Hydraul. Eng.*, 123(3), 1997, 237–243.
- [8] M.M. Rahman, N. Nagata, Y. Muramoto, and H. Murata, Effect of side slope on flow and scouring around spur-dike-like structures, *Proc., 7th Int. Symp. on River Sedimentation, Hong Kong, China, 1998*, 165–171.
- [9] N. Nagata, T. Hosoda, T. Nakato, and Y. Muramoto, Three-dimensional numerical model for flow and bed deformation around river hydraulic structures, *J. Hydraul. Eng.*, 131(12), 2005, 1074–1087.
- [10] C.J. Posey, Why bridges fail in floods, *Civ. Eng. (N.Y.)*, 19, 1949, 42–90.
- [11] H.W. Shen, V.R. Schneider, and S. Karaki, Local scour around bridge piers, *J. Hydraul. Div., Am. Soc. Civ. Eng.*, 95(6), 1969, 1919–1940.
- [12] B. Dargahi, Flow field and local scouring around a pier. Bulletin No. TRITA-VBI-137, Hydraulic Laboratory, Royal Institute of Technology, Stockholm, Sweden, 1988
- [13] A. J. Raudkivi, *Loose boundary hydraulics* (3rd Ed., Pergamon, New York, 1990).
- [14] F. Ahmed, and N. Rajaratnam, Flow around bridge piers, *J. Hydraul. Eng.*, 124(3), 1998, 288 – 300.
- [15] F. Ahmed, and N. Rajaratnam, Observations of flow around bridge abutment, *J. Eng. Mech.*, 126(1), 2000, 51 – 59.
- [16] B.W. Melville, Local scour at bridge abutments, *J. Hydraul. Eng., ASCE*, 118(4), 1992, 615–631.
- [17] W.S. Uijttewaala, D. Lehmann, and A. van Mazijk, Exchange processes between a river and its groyne fields: model experiments, *J. Hydraul. Eng., ASCE*, 127(11), 2001, 928–936.
- [18] V. Weitbrecht, W. Uijttewaala, and G.H. Jirka, 2D particle tracking to determine transport characteristics in rivers with dead zones, *Proc., Int. Symp. Shallow Flows, Delft, The Netherlands, 2009*, 103–110.
- [19] M.A. Stevens, M.M. Gasser, and M.B.A.M. Saad, Wake vortex scour at bridge piers, *J. Hydraul. Eng.*, 117(7), 1991, 891–904.
- [20] A. Chrisohoides, F. Sotiropoulos, and T.W. Sturm, Coherent structures in flat-bed abutment flow: computational fluid dynamics simulations and experiments, *J. Hydraul. Eng.*, 129(3), 2003, 177–186.
- [21] P.M. Biron, C. Robson, M.F. LaPointe, and S.J. Gaskin, Three-dimensional flow dynamics around deflectors, *River Research and Applications*, 21, 2005, 961–975.
- [22] T.W. Haltigin, P.M. Biron, and M.F. Lapointe, Predicting equilibrium scour-hole geometry near angled stream deflectors using a three-dimensional numerical flow model, *J. Hydraul. Eng.*, 133(8), 2007, 983–988.
- [23] C. Mendoza-Cabrales, Computation of flow past a cylinder mounted on a flat plate, *Proc., Hydraul. Eng., ASCE Reston, Va.*, 1993, 899–904.
- [24] J.E. Richardson, and V.G. Panchang, Three-dimensional simulation of scour-inducing flow at bridge piers, *J. Hydraul. Eng.*, 124(5), 1998, 530–540.
- [25] N.R.B. Olsen, and M.C. Melaan, Three-dimensional calculation of scour around cylinders, *J. Hydraul. Eng., ASCE*, 119(9), 1993, 1048–1054.
- [26] Y. Jia, and S.S.Y Wang, 3D numerical simulation of flow near a spur dike, *Adv. Hydrosoci.*, 1, 1993, 2150–2156.
- [27] R. Mayerle, F.M. Toro, and S.S.Y. Wang, Verification of a three-dimensional numerical model simulation of the flow in the vicinity of spur dikes, *J. Hydraul. Res.*, 33(2), 1995, 243–256.
- [28] S. Ouillon, and D. Dartus, Three-dimensional computation of flow around groyne, *J. Hydraul. Eng.*, 123(11), 1997, 962–970.
- [29] N.R.B Olsen, and H.M.K. Kjellesvig, Three-dimensional numerical flow modeling for estimation of maximum local scour depth, *J. Hydraul. Res.*, 36(4), 1998, 579–590.
- [30] A. Roulund, B.M. Sumer, J. Fredsoe, and J. Michelsen, 3D mathematical modeling of scour around a circular pile in current, *Proc., 7th Int. Symp. on River Sedimentation, Hong Kong, China, 1998*, 131–137.
- [31] H.D. Smith, and D.L. Foster, Modeling of flow around a cylinder over a scoured bed, *Journal of Waterway, Port, Coastal, and Ocean Engineering*, 131(1), 2005, 14–24.
- [32] T.M. Salaheldin, J. Imran, and H. Chaudhry, Numerical modeling of three-dimensional flow field around circular piers, *J. Hydraul. Eng.*, 130(2), 2004, 91–100.
- [33] R.I. Ferguson, D.R. Parsons, S.N. Lane, and R.J. Hardy, Flow in meander bends with recirculation at the inner bank, *Water Resour. Res.*, 39(11), 2003, 1322–1334.
- [34] K.F. Bradbrook, S.N. Lane, K.S. Richards, P.M. Biron, and A.G. Roy, Role of bed discordance at asymmetrical river confluences, *J. Hydraul. Eng.*, 127(5), 2001, 351–368.
- [35] H. Zhang, H. Nakagawa, T. Ishigaki, and Y. Muto, Prediction of 3D flow field and local scouring around spur dikes, *Ann. J. Hydraul. Eng.*, 49, 2005, 1003–1008.
- [36] A.R. Griffith, J.H. Rutherford, A. Alavi, D.D. Moore, and J. Groeneveld, Stability review of the Wanapum spillway using CFD analysis, *Bulletin, Canadian Dam Association.*, 2007, 16–26.

- [37] B.W. Melville, Local scour at bridge sites, Rep. No. 117, Dept. of Civil Engineering, School of Engineering., Univ. of Auckland, Auckland, New Zealand, 1975.
- [38] J. M. Sicilian, C.W. Hirt, and R.P. Harper, FLOW-3D: Computational modeling power for scientists and engineers. Rep. FSI-8700- 1, Flow Science, Los Alamos, N.M, 1987.
- [39] V. Yakhot, and S.A. Orszag, Renormalization group analysis of turbulence, J. Sci. Comp., 1(1), 1986, 3-12.
- [40] SonTek, Acoustic Doppler velocimeter (ADV) principles of operation, SonTek ADV Technical Manual, SonTek, San Diego, 2001.
- [41] Flow Science, Inc., FLOW-3D user's manual, 9.4 edition, Flow Science, Inc., Santa Fe, N.M., 2009.
- [42] W. Rodi, Turbulence models and their application in hydraulics: A state of the art Review, IAHR, 1980.
- [43] S.F. Bradford, Numerical simulation of surf zone dynamics, J. Waterw., Port, Coastal, Ocean Eng., 126(1), 2000, 1-13.
- [44] S.C. Chopakarla, A CFD model for wave transformations and breaking in the surf zone, MS Thesis, Ohio State University, Columbus, Ohio, 2003.
- [45] C.W. Hirt, and J.M. Sicilian, A porosity technique for the definition of obstacles in rectangular cell meshes. Proc., 4th Int. Conf. Ship Hydrodynamics, Washington, D.C., 1985.
- [46] B.E. Launder, and D.B. Spaulding, Mathematical models of turbulence (Academic Press, New York, N.Y., 1972).
- [47] M. Abbot, and D. Basco, Computational Fluid Dynamics: An Introduction for Engineers (Longman Publishing Group, 1989, ISBN-10: 0582013658).
- [48] C.T Shaw, Using computational fluid dynamics. (Prentice Hall, New York, N.Y., 1992).
- [49] V. Yakhot, S.A. Orszag, S. Thangam, T.B. Gatschi, and C.G. Speziale, Development of a turbulence model for shear flow by a double expansion technique, Phys. Fluids A, 4(7), 1992, 1510-1520.
- [50] M.A. Yaeger, Mean flow and turbulence around two series of experimental dikes, MS Thesis, Department of Hydrology and Water Resources, University of Arizona, Tucson, AZ, 100 pp., 2009.
- [51] P.M. Biron, T.W. Haltigin, R.J. Hardy, and M.F. Lapointe, Assessing different methods of generating a three-dimensional numerical model mesh for a complex stream bed topography, Int. J. Comput. Fluid Dyn., 21(1), 2007, 37-47.
- [52] K.F. Bradbrook, P.M. Biron, S.N. Lane, K.S. Richards, and A.G. Roy, Investigation of controls on secondary circulation in a simple confluence geometry using a three-dimensional numerical model, Hydrol. Processes, 12, 1998, 1371-1396.
- [53] A. Hodkinson, and R.I. Ferguson, Numerical modeling of separated flow in river bends: Model testing and experimental investigation of geometric controls on the extent of flow separation at the concave bank, Hydrol. Processes, 12, 1998, 1323-1338.
- [54] S.N. Lane, K.F. Bradbrook, K.S. Richards, P.A. Biron, and A.G. Roy, The application of computational fluid dynamics to natural river channels: three-dimensional versus two-dimensional approaches, Geomorphology, 29, 1999, 1-20.
- [55] A.P. Nicholas, and G.H.S. Smith, Numerical simulation of three-dimensional flow hydraulics in a braided channel, Hydrol. Processes, 13, 1999, 913-929.
- [56] K.F. Bradbrook, S.N. Lane, and K.S. Richards, Numerical simulation of three-dimensional, time-averaged flow structure at river channel confluences, Water Resour. Res., 36, 2000a, 2731-2746.
- [57] V. Yakhot, and L.M. Smith, The renormalization group, the eps-expansion and derivation of turbulence, J. Sci. Comp., 7(1), 1992, 35-61.

Notations

The following symbols are used in this paper:

x = horizontal longitudinal direction	L = weir crest length (cm)
y = horizontal transverse direction	l = dike length (cm)
z = vertical direction	V_x = velocity in horizontal direction ($m \cdot s^{-1}$)
h = depth of water at the weir (m)	u, v, w = mean flow velocities ($m \cdot s^{-1}$)
H = height of water flowing over the weir (m)	u_* = shear velocity ($m \cdot s^{-1}$)
D = distance between two dikes at the base (cm)	ρ = density of water ($kg \cdot m^{-3}$)
Q = volumetric discharge ($m^3 \cdot s^{-1}$)	K = weir constant for discharge units $m^3 \cdot hr^{-1}$